

Supporting information

Scalable Assembly of Crystalline Binary Nanocrystal Superparticles and Their Enhanced Magnetic and Electrochemical Properties

Yuchi Yang,^{†,‡} Biwei Wang,[‡] Xiudi Shen,[†] Luyin Yao,[†] Lei Wang,[†] Xiao Chen,[†]

Songhai Xie,[‡] Tongtao Li,[‡] Jianhua Hu,[†] Dong Yang,[†] and Angang Dong^{*,‡}

[†]State Key Laboratory of Molecular Engineering of Polymers and Department of Macromolecular Science, Fudan University, Shanghai 200433, China.

[‡]*iChem*, Shanghai Key Laboratory of Molecular Catalysis and Innovative Materials, and Department of Chemistry, Fudan University, Shanghai 200433, China.

*To whom correspondence should be addressed: agdong@fudan.edu.cn (A.D.)

Table of Contents

Figure S1. TEM images and the corresponding size distribution histograms of 8.0 nm CoFe ₂ O ₄ NCs and 17.0 nm Fe ₃ O ₄ NCs.....	S3
Figure S2. The different lattice planes of AB ₁₃ -type CoFe ₂ O ₄ -Fe ₃ O ₄ binary superparticles	S4
Figure S3. The defects of AB ₁₃ -type CoFe ₂ O ₄ -Fe ₃ O ₄ binary superparticles	S5
Figure S4. TEM images of 8.5 nm and 17.0 nm Fe ₃ O ₄ NCs	S6
Figure S5. DLS measurements of AB ₁₃ -type Fe ₃ O ₄ -Fe ₃ O ₄ BNSL colloids.....	S7
Figure S6. SEM images of single-component superparticles self-assembled from 17.0 nm Fe ₃ O ₄ NCs.....	S8
Figure S7. TEM images of AlB ₂ -type binary superparticles with various sizes.....	S9
Figure S8. TEM image and corresponding SAXS pattern of AlB ₂ -type binary superparticles and core-shell superparticles.....	S10
Figure S9. TEM images of Pd-Fe ₃ O ₄ and Au-Fe ₃ O ₄ binary superparticles	S11
Figure S10. TEM image and the corresponding SAXS patterns of AB ₁₃ -type CoFe ₂ O ₄ -Fe ₃ O ₄ binary superparticles self-assembled with different surfactants.....	S12
Figure S11. SEM images and SAXS patterns of <i>fcc</i> superparticles.....	S13
Figure S12. TEM images and the corresponding SAXS patterns of various superparticles after ligand carbonization	S14
Figure S13. Representative CV curves of <i>fcc</i> superparticles composed of 17.0 nm Fe ₃ O ₄ NCs and 8.0 nm CoFe ₂ O ₄ NCs.....	S15
Figure S14. Cross-sectional illustration depicting the structural evolution during electrochemical lithiation.....	S16
Table S1. Reaction conditions for monodisperse Fe ₃ O ₄ NCs with different sizes...	S17
Table S2. NC formulation for the growth of various BNSL colloids.....	S18
Table S3. Fe and Co contents in the electrolyte after cycling	S19
Calculation of the packing fraction of binary superparticles	S20

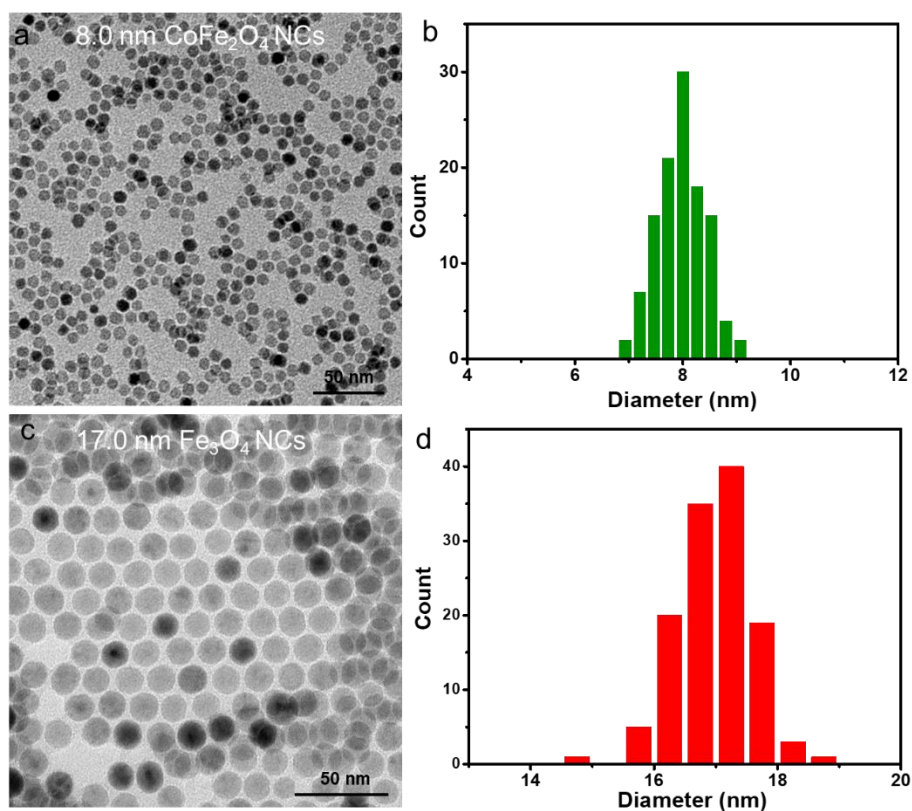


Figure S1. TEM images and the corresponding size distribution histograms of (a, b) 8.0 nm CoFe_2O_4 NCs and (c, d) 17.0 nm Fe_3O_4 NCs used for constructing AB_{13} -type binary superparticles.

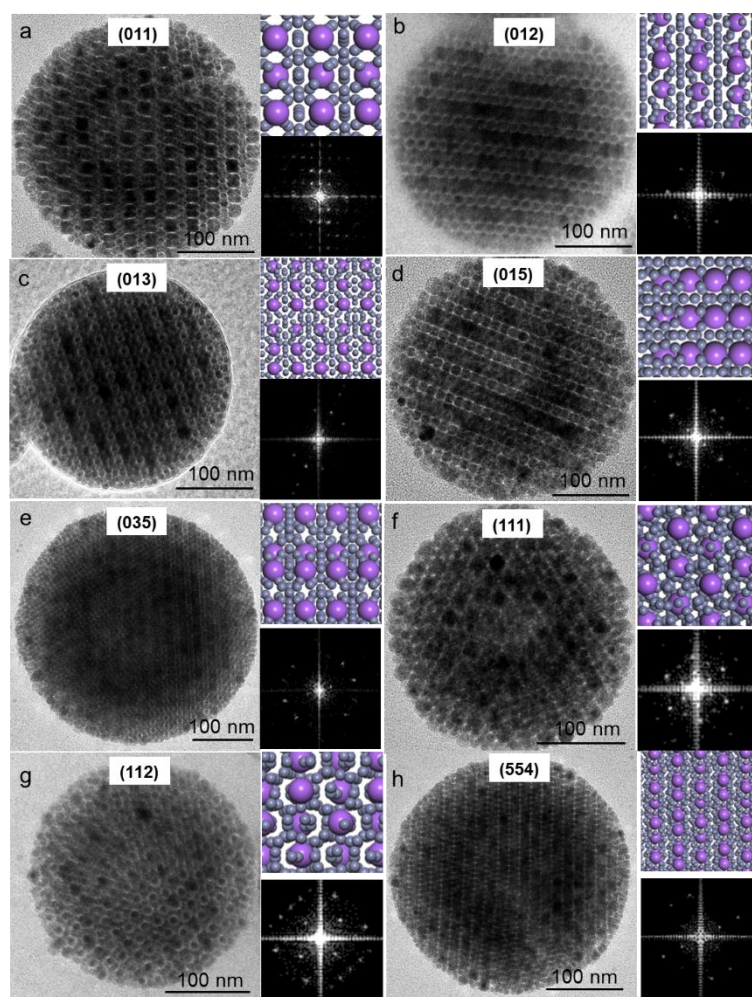


Figure S2. (a-h) TEM images and the corresponding crystallographic models and FFTs of AB₁₃-type CoFe₂O₄-Fe₃O₄ binary superparticles viewed from various lattice planes as indicated.

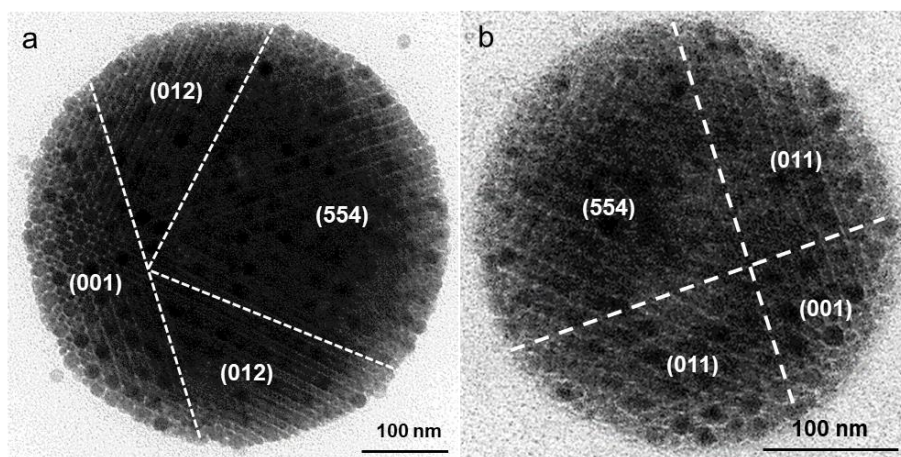


Figure S3. (a, b) TEM images of AB₁₃-type CoFe₂O₄-Fe₃O₄ binary superparticles with grain boundaries.

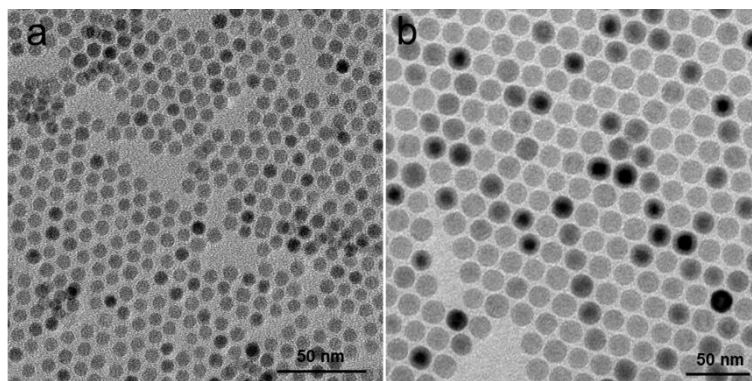


Figure S4. TEM images of (a) 8.5 nm and (b) 17.0 nm Fe_3O_4 NCs used for constructing AB_{13} -type Fe_3O_4 - Fe_3O_4 binary superparticles.

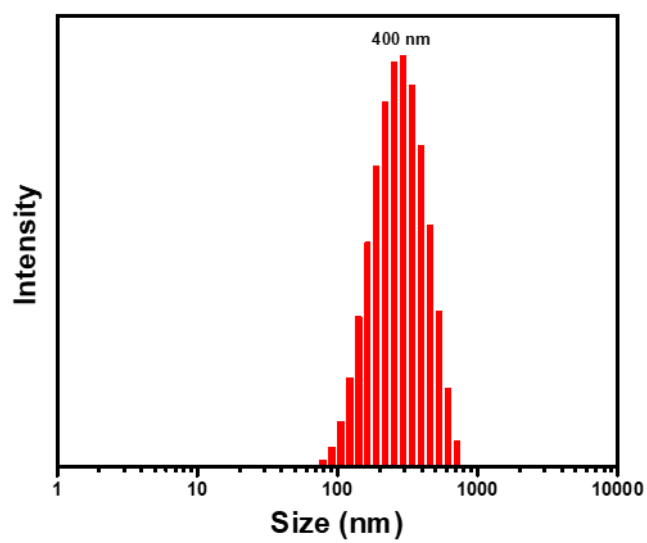


Figure S5. DLS measurements of AB₁₃-type Fe₃O₄-Fe₃O₄ BNSL colloids.

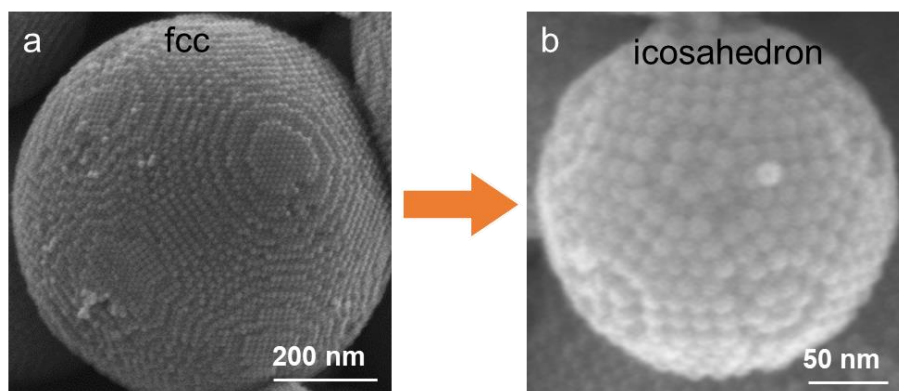


Figure S6. SEM images of single-component superparticles self-assembled from 17.0 nm Fe_3O_4 NCs, showing the transition from (a) *fcc* to (b) icosahedral symmetry as the superparticle size is reduced to ~ 200 nm.

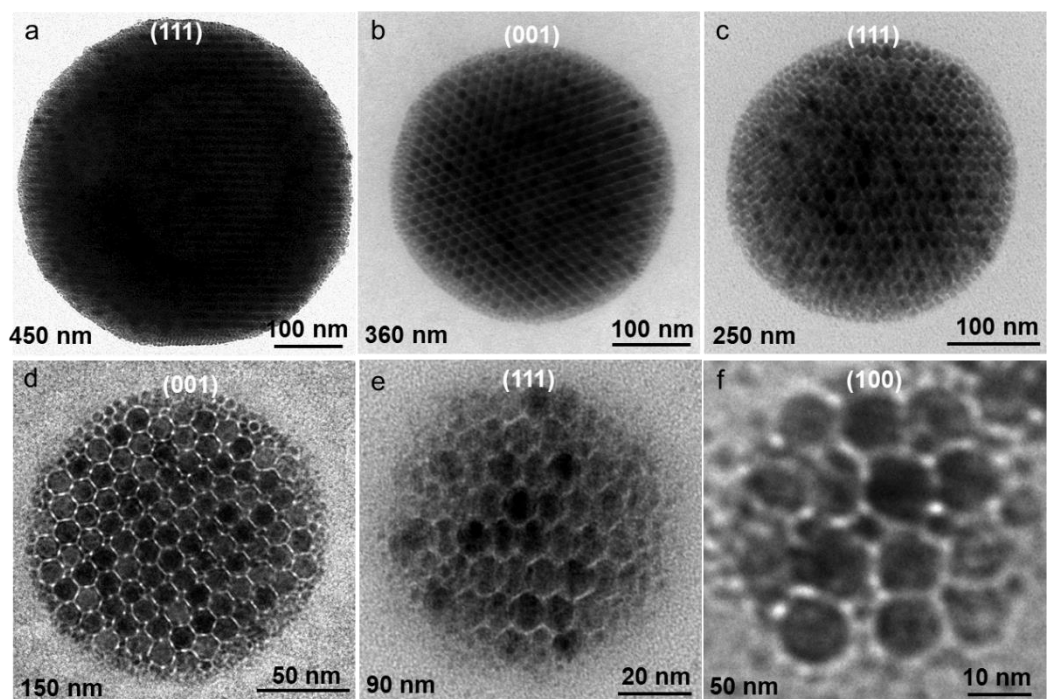


Figure S7. TEM images of a series of AlB₂-type binary superparticles with sizes gradually decreasing from 450 to 50 nm.

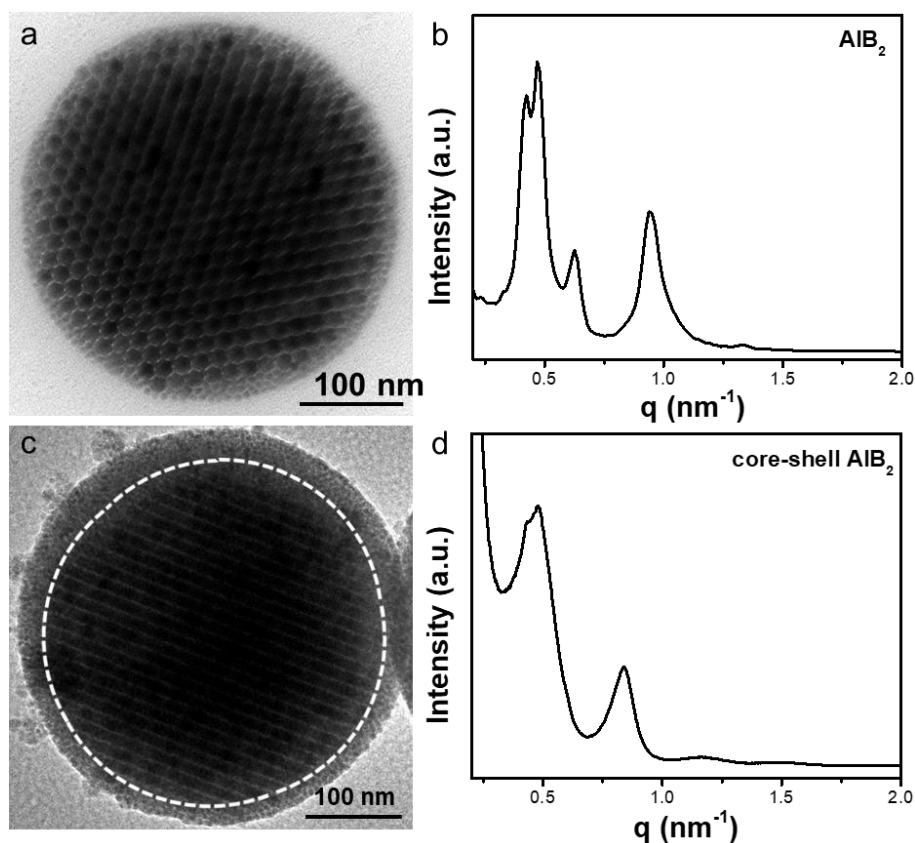


Figure S8. (a, b) TEM image and corresponding SAXS pattern of AlB_2 -type binary superparticles self-assembled from 4.5 nm CoFe_2O_4 NCs and 11.0 nm Fe_3O_4 NCs with a number ratio of $\sim 2:1$. (c, d) TEM image and corresponding SAXS pattern of core-shell superparticles featuring AlB_2 -type cores (as indicated by the dashed circle), which were self-assembled from 4.5 nm CoFe_2O_4 NCs and 11.0 nm Fe_3O_4 NCs with a number ratio of $\sim 13:1$.

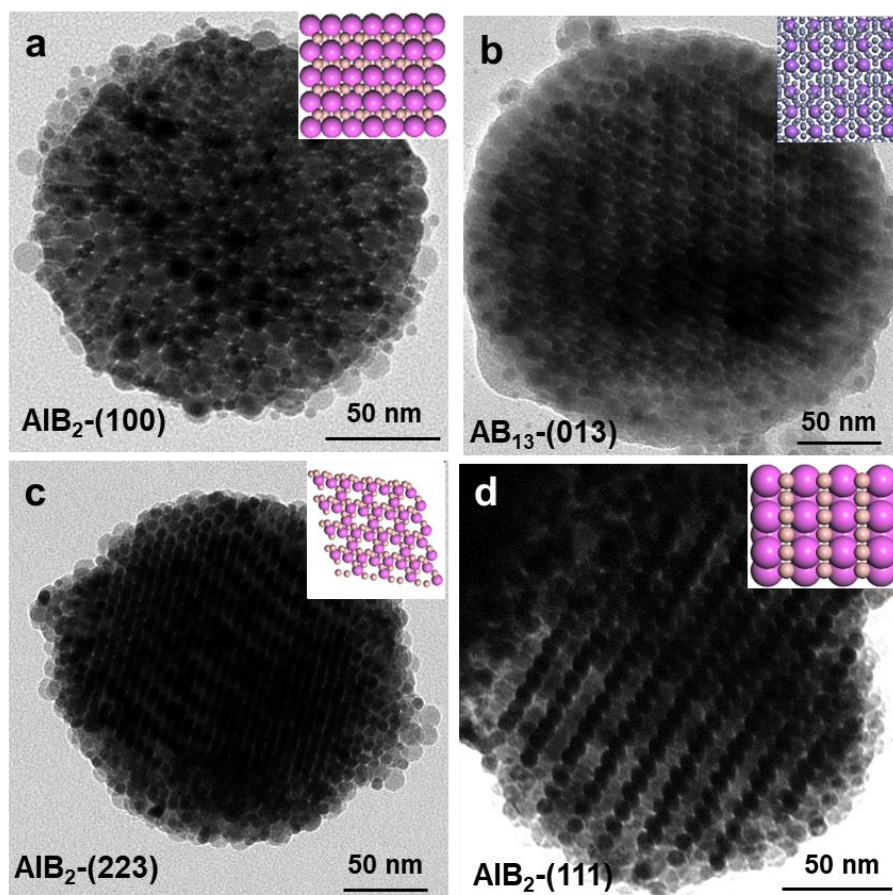


Figure S9. TEM images of binary superparticles with various structures and compositions: (a) AlB_2 -type superparticles composed of 6.0 nm Pd NCs and 15.0 nm Fe_3O_4 NCs; (b) AB_{13} -type superparticles composed of 8.0 nm Pd NCs and 15.0 nm Fe_3O_4 NCs; (c) AlB_2 -type superparticles composed of 7.0 nm Au NCs and 15.0 nm Fe_3O_4 NCs onto the (223) lattice plane; (d) AlB_2 -type superparticles composed of 7.0 nm Au NCs and 15.0 nm Fe_3O_4 NCs onto the (111) lattice plane. Insets show the corresponding crystallographic models.

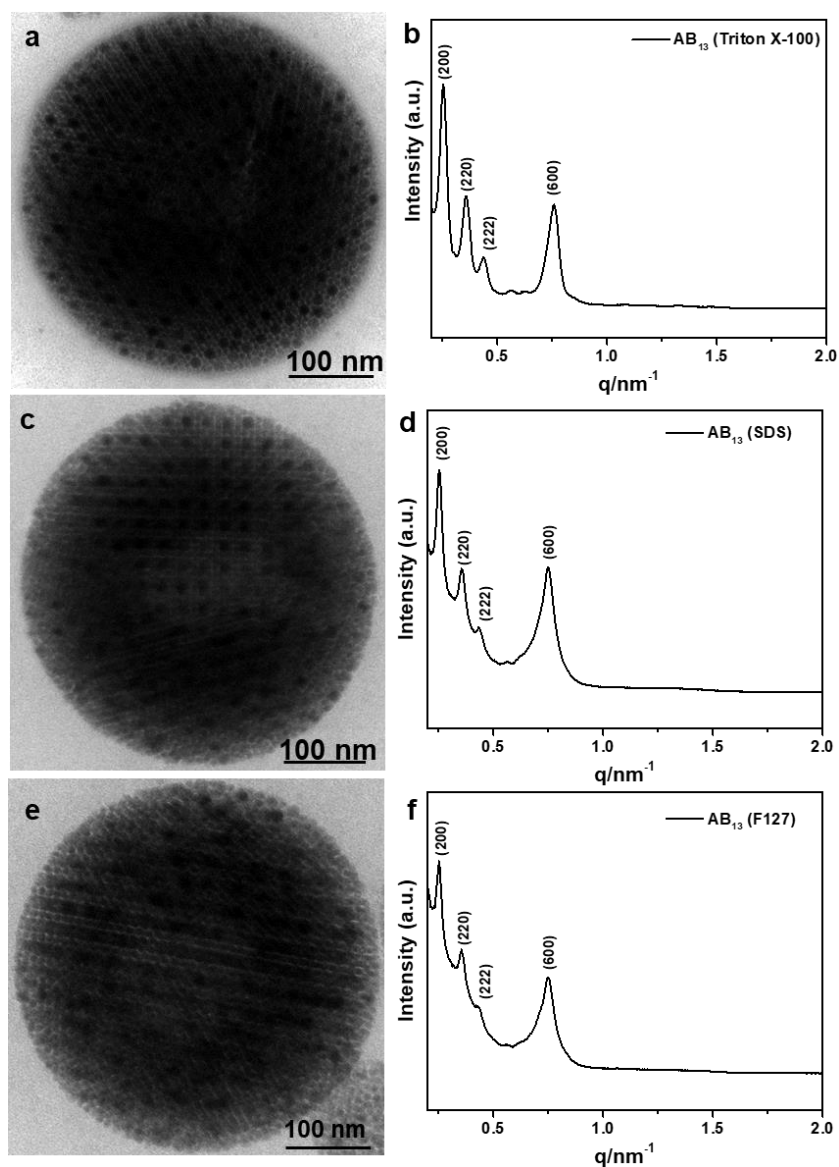


Figure S10. TEM image and the corresponding SAXS patterns of AB_{13} -type $CoFe_2O_4$ - Fe_3O_4 binary superparticles self-assembled with the assistance of different surfactants: (a, b) Triton X-100, (c, d) SDS, and (e, f) F127.

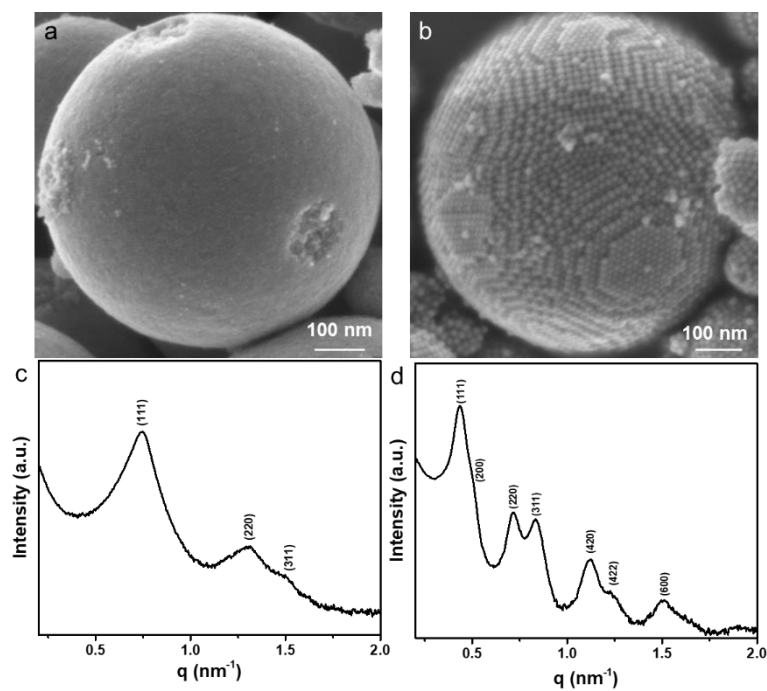


Figure S11. SEM images and the corresponding SAXS patterns of *fcc* superparticles composed of (a, c) 8.0 nm CoFe_2O_4 NCs and (b, d) 17.0 nm Fe_3O_4 NCs.

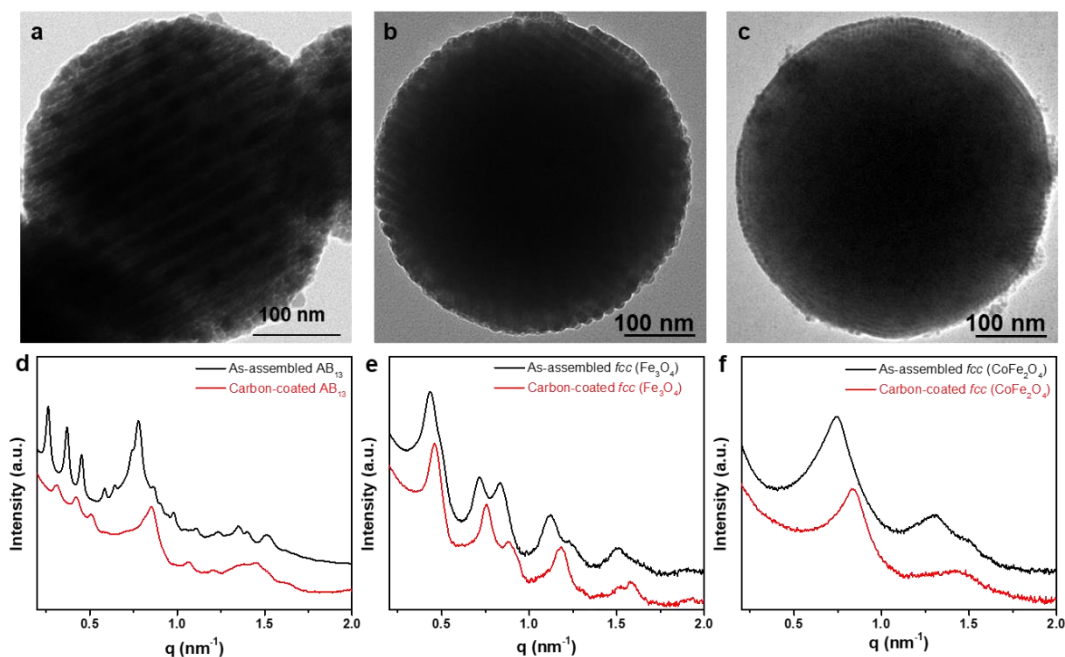


Figure S12. TEM images and the corresponding SAXS patterns of various superparticles after ligand carbonization: (a, d) carbon-coated AB_{13} -type binary superparticles composed of 8.0 nm $CoFe_2O_4$ and 17.0 nm Fe_3O_4 NCs; (b, e) carbon-coated *fcc* superparticles of 17.0 nm Fe_3O_4 NCs; (c, f) carbon-coated *fcc* superparticles of 8.0 nm $CoFe_2O_4$ NCs. For each type of superparticles, the SAXS patterns before ligand carbonization were also provided in (d-f) for comparison. For all sample, the peaks were systematically shifted toward high angles after ligand carbonization, suggesting the occurrence of lattice contract.

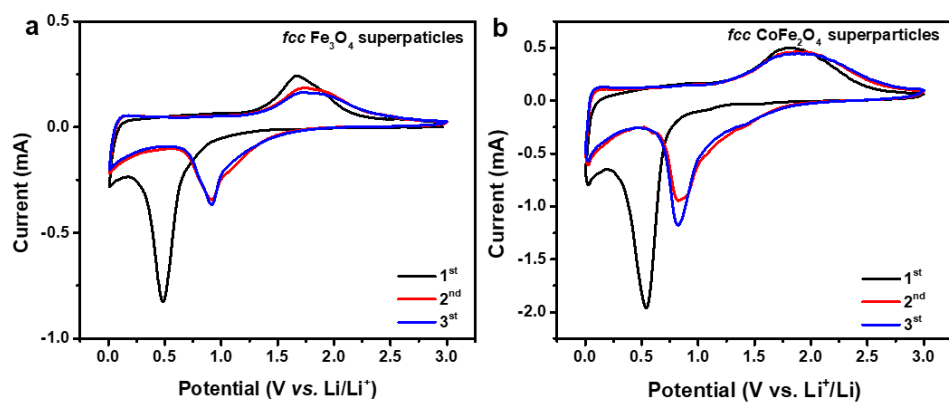


Figure S13. Representative CV curves of *fcc* superparticles composed of (a) 17.0 nm Fe_3O_4 NCs and (b) 8.0 nm CoFe_2O_4 NCs, respectively.

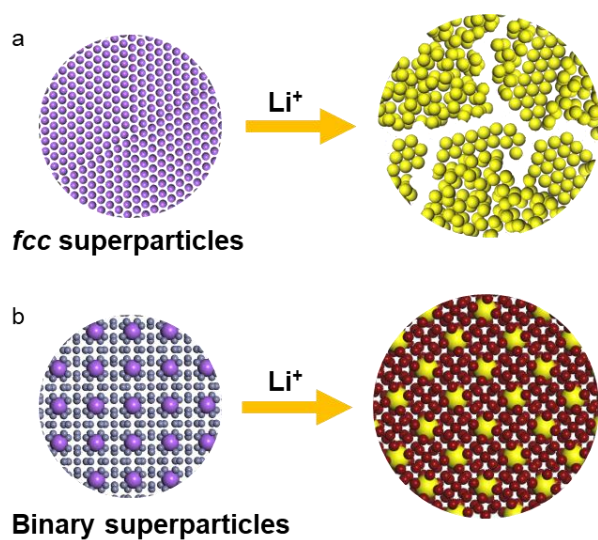


Figure S14. Cross-sectional illustration depicting the structural evolution of (a) *fcc* superparticles and (b) binary superparticles during electrochemical lithiation.

Table S1. Reaction conditions for growing monodisperse Fe₃O₄ NCs with different sizes.

NC size	Solvent	Fe(OA) ₃	OA	Temperature (°C)
20.0 nm	50 g ODE	9.0 g	2.0 g	325
17.0 nm	50 g ODE	9.0 g	2.0 g	320
15.0 nm	50 g ODE	9.0 g	2.0 g	318
11.0 nm	10 g TDE/40 g ODE	9.0 g	2.0 g	300
9.0 nm	17.5 g TDE/32.5 g ODE	9.0 g	1.5 g	290
8.5 nm	50 g HDE	9.0 g	2.0 g	290
7.0 nm	50 g HDE	9.0 g	2.0 g	288
6.5 nm	10 g TDE/40 g HDE	9.0 g	2.0 g	280

Table S2. NC formulation for the growth of various BNSL colloids (The concentration of all NCs is 75 mg mL⁻¹ unless noted).

Lattice structure	Volume of large NCs	Volume of small NCs
AB ₁₃	8.0 mL 17.0 nm Fe ₃ O ₄	12.0 mL 8.0 nm CoFe ₂ O ₄
AB ₁₃	8.0 mL 17.0 nm Fe ₃ O ₄	12.0 mL 8.5 nm Fe ₃ O ₄
AB ₁₃	8.0 mL 20.0 nm Fe ₃ O ₄	12.0 mL 9.0 nm CoFe ₂ O ₄
AlB ₂	15.0 mL 11.0 nm Fe ₃ O ₄	5.0 mL 4.5 nm CoFe ₂ O ₄
AlB ₂	15.0 mL 15.0 nm Fe ₃ O ₄	5.0 mL 7.0 nm Fe ₃ O ₄
MgZn ₂	12.0 mL 6.5 nm Fe ₃ O ₄	8.0 mL 4.5 nm CoFe ₂ O ₄
MgZn ₂	12.0 mL 9.0 nm Fe ₃ O ₄	8.0 mL 6.5 nm Fe ₃ O ₄
NaCl	19.0 mL 15.0 nm Fe ₃ O ₄	1.0 mL 4.5 nm CoFe ₂ O ₄
CaCu ₅	9.0 mL 7.0 nm Fe ₃ O ₄	11.0 mL 4.5 nm CoFe ₂ O ₄
AB ₁₃	0.2 mL 15.0 nm Fe ₃ O ₄	0.8 mL 8.0 nm Pd (20 mg mL ⁻¹)
AlB ₂	0.45 mL 15.0 nm Fe ₃ O ₄	0.55 mL 6.0 nm Pd (20 mg mL ⁻¹)
AlB ₂	0.25 mL 15.0 nm Fe ₃ O ₄	0.75 mL 7.0 nm Au (20 mg mL ⁻¹)

Table S3. The leached Fe and Co contents in the electrolyte after cycling.

Anodes	Fe (ppm)	Fe mass loss percentage (%)	Co (ppm)	Co mass loss percentage (%)
AB ₁₃ binary superparticles	70	1.7	4	0.3
<i>fcc</i> CoFe ₂ O ₄ superparticles	172	4.8	28	1.5
<i>fcc</i> Fe ₃ O ₄ superparticles	442	8.3	None	None

Calculation of the packing fraction of carbon-coated AB₁₃-type CoFe₂O₄-Fe₃O₄ binary superparticles

1. Determination of the carbon shell thickness in fcc superparticles of 17.0 nm Fe₃O₄

NCs:

According to SAXS, the lattice constant (a) of fcc superparticles of 17.0 nm Fe₃O₄ NCs

is calculated to be $a = \frac{2\pi\sqrt{h^2+k^2+l^2}}{q} = 24.6$ nm, where h , k , and l are Miller's indices and q

is the scattering vector.

The volume of a unit cell, $Volume_{(\text{unit cell})}$, is calculated as below:

$$Volume_{(\text{unit cell})} = a^3 = (24.6 \text{ nm})^3 = 14887 \text{ nm}^3.$$

Since the theoretical packing fraction of fcc superparticles is 74%, the carbon shell thickness ($L1$) surrounding individual Fe₃O₄ NCs is calculated to be 0.2 nm by the

equation $\frac{Volume(\text{NC} + \text{carbon shell})}{Volume(\text{unit cell})} = \frac{4\pi}{3} \times \frac{4(8.5+L1)^3}{14887} = 74\%$.

2. Determination of the carbon shell thickness in fcc superparticles of 8.0 nm CoFe₂O₄

NCs:

According to SAXS, the lattice constant (a) of fcc superparticles of 8.0 nm CoFe₂O₄

NCs is calculated to be $a = \frac{2\pi\sqrt{h^2+k^2+l^2}}{q} = 11.9$ nm.

The volume of a unit cell, $Volume_{(\text{unit cell})}$, is calculated as below:

$$Volume_{(\text{unit cell})} = a^3 = (11.9 \text{ nm})^3 = 1685 \text{ nm}^3.$$

Similar to fcc Fe₃O₄ superparticles, the carbon shell thickness $L2$ is calculated to be 0.2

nm by the equation $\frac{Volume(\text{NCs} + \text{carbon shell})}{Volume(\text{unit cell})} = \frac{4\pi}{3} \times \frac{4(4.0+L2)^3}{1685} = 74\%$

3. Calculation of the packing fraction of carbon-coated AB₁₃ superparticles:

According to SAXS, the lattice constant (a) of AB₁₃-type CoFe₂O₄-Fe₃O₄ binary

superparticles is calculated to be $a = \frac{2\pi\sqrt{h^2+k^2+l^2}}{q} = 42.9$ nm.

The volume of a unit cell, $Volume_{(\text{unit cell})}$, is calculated as below:

$$Volume_{(\text{unit cell})} = a^3 = (42.9 \text{ nm})^3 = 78954 \text{ nm}^3.$$

Assuming that the carbon shells surrounding 17.0 nm Fe_3O_4 NCs and 8.0 nm CoFe_2O_4 NCs in binary superparticles are the same as $L1$ and $L2$ in thickness, the packing fraction of carbon-coated AB_{13} superparticles can be calculated as below:

$$packing\ fraction = \frac{Volume\ (\text{NCs} + \text{carbon shell})}{Volume\ (\text{unit cell})} = \frac{4\pi}{3} \times \frac{8(8.5+L1)^3 + 104(4.0+L2)^3}{78954} = 69\%.$$